ACADEMIA ROMÂNĂ
Revue Roumaine de Chimie
https://www.icf.ro/rrch/

Rev. Roum. Chim.,
2025, *70*(1–2), 53–63
DOI: 10.33224/rrch.2025.70.1-2.05

FABRICATED A NOVEL MAGNETIC HYDROGEL NANOCOMPOSITE FROM XANTHAN GUM FOR REMOVAL OF Cu(II) FROM WATER AND WASTE WATER SAMPLES

Narges SALEHI,[a] Ali MOGHIMI[*, a] and Hossein ANARAKI-ARDAKANI[*, b]

[a]Department of Chemistry, Faculty of Pharmaceutical Chemistry, Tehran Medical Sciences, Islamic Azad University, Tehran, Iran
[b]Department of Chemistry, Karaj Branch, Islamic Azad University, Karaj, Iran

Received September 3, 2024

Following industrialization and urbanization, water pollution by heavy metals is the most important environmental problem in the world, therefore, today, water and wastewater treatment to remove heavy metals has received more attention to reduce serious risks for humans and living organisms. In the present study, A novel magnetic hydrogel nanocomposite was synthesized by modifying Xanthan Gum (XG) with polyacrylamide and polyacrylic acid as homopolymer and magnetic iron oxide nanoparticles (MNPs Fe_3O_4) for the removal of Cu(II) from water and wastewater samples. The magnetic hydrogel nanocomposite was characterized by Fourier-transform infrared spectroscopy (FT-IR), X-ray diffraction (XRD), and scanning electron microscopy (SEM). The relevant parameters on adsorption were optimized. Isotherm models were studied and the maximum adsorption capacities of Cu (II) was 160.2 mg/g and the adsorption proses controlled by pseudo-second-order kinetic. Finally, the magnetic hydrogel nanocomposite exhibited high performance for the removal of Cu(II) from water and waste water samples.

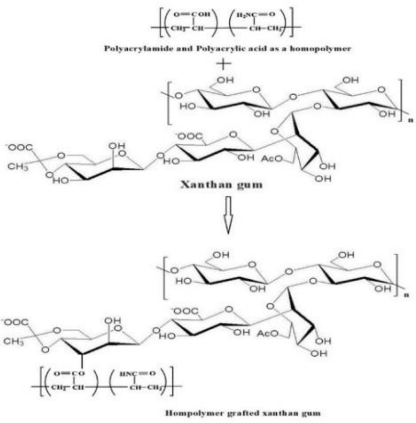

INTRODUCTION

Heavy metals are one of the most threatening pollutants in water systems, so water pollution by heavy metals is known as one of the most important environmental problems in the world.[1] Lack of water and high water consumption have forced people to maintain the quality of water resources. Therefore, wastewater treatment is essential to keep the quality of water resources.[2] For example, it is well known that copper (Cu) has comprehensive industrial sources and various biological toxicity and may cause gastrointestinal illness, vomiting, or even death.[3] As a result, there is a need to develop simple yet very effective techniques to remove heavy metal ions from wastewater. These include chemical precipitation, photocatalysis, adsorption, reverse osmosis, electrodialysis, membrane filtration, etc.[4,5]

In the meantime, adsorption has received much attention as an efficient method due to its simplicity, cost-effectiveness, environmental friendliness by releasing no harmful byproducts, and high efficiency. Also, the development of cost-effective adsorbents with good adsorption capacity and good reusability has created the research field of many researchers.[5] Compatibility with the environment is

* Corresponding authors: alimoghimi@iauvaramin.ac.ir; kamran9537@yahoo.com; Ali.Moghimi@iaups.ac.ir (A.M.); hosseinanaraki@yahoo.com (H.A.A.)

one of the critical characteristics of natural polymers. Therefore many studies have been conducted to develop these cheap and efficient adsorbents.[6] Biomaterial-based hydrogels have been considered for wastewater treatment due to their renewable nature, environmental compatibility, and hydrophilic network of cross-linked polymers.[6] Various biological materials such as starch, cellulose, alginate, silk fibroin, guar gum, xanthan and chitosan are used to make these hydrogel-based absorbents.[7] These adsorbents are readily available, have biodegradable functional groups containing oxygen on their surfaces, and are non-toxic.[7,8] The Xanthan Gum (XG) is a polysaccharide biopolymer produced from non-toxic and biodegradable.[9] XG has an anionic character due to its glucuronic acid and pyruvic acid side chains.[8,10] In the molecular structure of its main and side chain, there are many carbonyl and hydroxyl groups that adsorb water-soluble pollution through hydrogen bonds and van der Waals forces.[6] Unique rheological properties, high solubility in water, presence of active functional groups throughout its chain, stability against heat, acids and bases increase its use in water purification.[9] Relatively low surface area, poor mechanical strength and low adsorption efficiency are disadvantages of XG, which can be overcome by combining nanoparticles, monomers, composition of some mineral nanofiller in the XG network.[11,12] Magnetic iron oxide nanoparticles (MNPs Fe_3O_4) have been widely used due to their petite size and high surface-to-volume ratio. On the other hand, they are easily and quickly separated from the solution by induction of a magnetic field.[13]

In this study, xanthan-based hydrogel was synthesized to remove copper from wast water. XG as a cost-effective and biocompatible stable polymer was used as the main component of the hydrogel. After synthesizing the adsorbent by modifying XG with Fe_3O_4 nanoparticles and polyacrylamide and polyacrylic acid as a homopolymer, the functional groups of XG, improve its mechanical resistance and surface area, copper was determined using Graphite furnace-atomic absorption spectrometer (GF-AAS, Varian, SPECTRA AA200, Australia). On the other hand, due to the magnetism of the adsorbent, it was very easily and quickly separated to separate the solution by induction of a magnetic field. Also, the adsorbent was characterized by FT-IR, XRD and SEM and the effective parameters on Cu(II) adsorption were optimized using the proposed method. The experimental data were fitted with the Langmuir isotherm model and the pseudo-first-order kinetic model. Also, thermodynamic parameters for Cu(II) adsorbed on the adsorbent was calculated. Finally, the results showed that the proposed method is simple, rapid, biocompatible, cost-effective and potentially valuable for copper removal in wastewater samples.

EXPERIMENTAL

1. Reagents

XG, acrylic acid (AA), acrylamide (AAm), potassium persulphate (KPS) and ascorbic acid (ABC), N'-methylene-bis-acrylamide (MBA), provided from Sigma Aldrich. Copper(II) nitrate trihydrate($Cu(NO_3)_2.3H_2O$) (purity > 99.5%) and MNPs Fe_3O_4 with size < 20 nm with purity 99.5%, were prepared from Merck (Darmstadt, Germany). The stock solution of Cu(II) (1000 mg/L) was prepared by dissolving an appropriate amount of the salt in 1000 ml of deionized water, and the working solution was prepared in doubly distilled water by suitable diluting for batch experiments using deionized water.

2. Synthesis of the magnetic hydrogel nanocomposite

For 4 hours, 50 mg of magnetic nanoparticles were sonicated at 20°C ml of deionized water. 1.0 g XG to the dispersed mixture was added and thoroughly stirred, and 30mg KPS and 20 mg of ABC were added to initiate the graft copolymerization process at 60 °C. 50 mg MBA was also added to the reaction mixture with stirring. 2.5 mL of AA and 1 g of AAm were slowly added while stirring.

The reaction continued for 3 hours. After that, the product was cooled to room temperature. Then polyacrylamide and Polyacrylic acid as a homopolymer in the synthesized magnetic hydrogel nanocomposite were removed using soxhlet extraction with acetone for about 5–6 hours. The rest of the homopolymers were separated by stirring the hydrogel nanocomposite in acetone for about 24 hours using a magnetic stirrer.[13] Finally, the synthesized magnetic hydrogel nanocomposite was dried and powdered in an oven with hot air at 60 °C (Scheme 1).

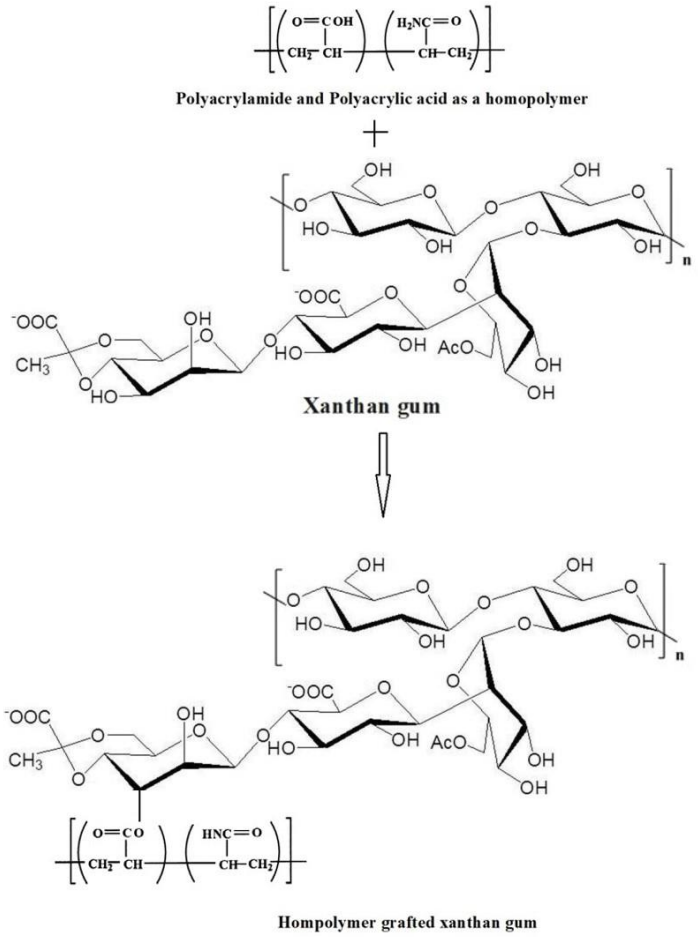

Scheme 1 – Synthesis of magnetic hydrogel nanocomposite.

3. Removal of Cu(II) from aqueous solutions

2 mL of the acetate buffer solution was added to 100 mL of the 20 mL Cu(II) solution to adjust the pH to 6. Then 5 mg of magnetic hydrogel nanocomposite was added to it and mixed for 60 minutes on a shaker at a speed of 120 rpm. After getting equilibrium mode, the hydrogel nanocomposite was separated from the Cu(II) solution by a magnet. Then the concentration of Cu(II) in sample solution was determined by Graphite furnace-atomic (GF-AAS, Varian, SPECTRA AA200, Australia) and using the calibration curve.

The adsorption efficiency of magnetic hydrogel nanocomposite for the adsorption of Cu(II) was calculated by the equation (1):[14,15]

$$\%\, Removal = ((C_0 - C_e)/C_0) \times 100 \quad (1)$$

where, C_0 is initial concentration of Cu(II) (mg/L) and C_e is equilibrium concentration of Cu(II), respectively (mg/L).

The capacity in equilibrium sorption (q_e (mg/g)) was obtained from the equation (2):

$$q_e = V(C_0 - C_e)/W \quad (2)$$

where C_e and C_0 are the equilibrium and initial concentration of Cu(II) (mgL^{-1}), respectively. V is the volume (L) of the Cu(II) and W (g) is sorbent mass.[16,17]

RESULTS AND DISCUSSION

1. Characterization of the adsorbent

1.2. IR spectra analysis

The FTIR spectrums were recorded by using an FTIR spectrometer (Thermo, AVATAR, Massachusetts, USA) in the range 4000–400 cm^{-1}. FTIR spectra of Fe_3O_4 and magnetic hydrogel nanocomposite are shown in Figs. 1a and b. In Fig. 1a, the peak at 575.86 cm^{-1} due to stretching

vibration of Fe–O. After coating Fe_3O_4 and synthesizing the magnetic hydrogel nanocomposite, the stretching vibration of Fe–O was shifted to 598.97 cm^{-1}(Figure1b). In Figure 1b, which is related to the magnetic hydrogel nanocomposite, the peaks at 3413.98 cm^{-1} and 2909.93 cm^{-1} are related to the –OH stretching vibration of carbohydrate and acrylic acid, respectively.[17–19] Two peaks at 1732.15 cm^{-1} and 1615.74 cm^{-1} due to C=O and –CO stretching vibrations, respectively.

Additionally, peaks at 1417.52 cm^{-1} and 1275.68 cm^{-1} correspond respectively to NH and CN stretching bond, and the peak at 792.17 cm^{-1} probably due to characteristic peaks of XG.[20,21] The results showed evidence of successful copolymerization on XG and uniform distribution of Fe_3O_4 in the magnetic hydrogel nanocomposite.

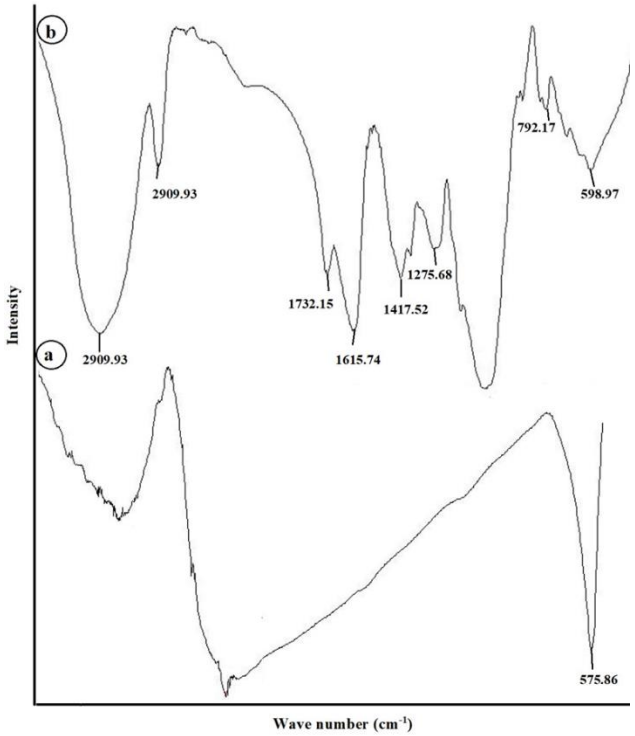

Fig. 1 – (a) – FTIR spectra of Fe_3O_4 and (b**)**- FTIR spectra of magnetic hydrogel nanocomposite.

1.3. X-ray diffraction analysis

The XRD pattern of Fe_3O_4 and the magnetic hydrogel nanocomposite presented in Fig. 2. In the XRD pattern of Fe_3O_4, diffraction peaks were shown at 2θ = 30.1°, 35.6°, 43.2°, 53.6° and 62.6°, labeled by their indicators ((220), (311), (400), (422), (511), and (440)). These peaks also were appeared in the XRD pattern of magnetic hydrogel nanocomposite but with a little less intense. The XRD data showed evidence of successful Fe_3O_4 coated with XG copolymerized.

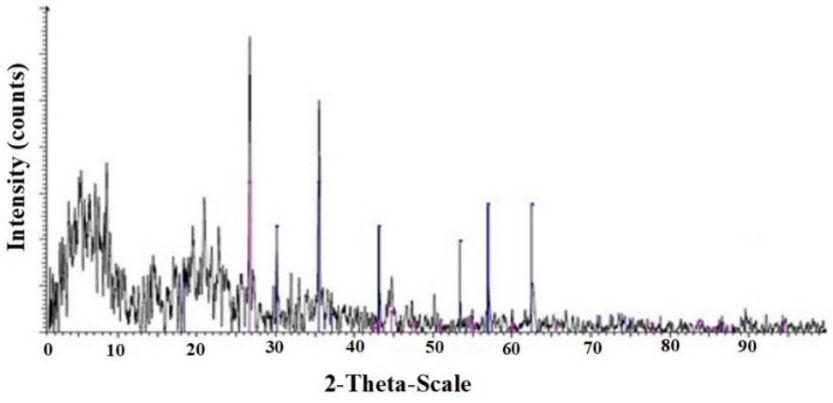

Fig. 2 – XRD pattern of Fe_3O_4 and the magnetic hydrogel nanocomposite.

1.4. SEM analysis

The morphology of the magnetic hydrogel nanocomposite was investigated by scanning electron microscope (SEM, PHILIPS, CM120, Amsterdam, Netherlands). The SEM image of the hydrogel nanocomposite is presented in Fig. 3. As seen in Fig. 3, as can be seen in the figure, the particles are irregular polygonal shapes and partially accumulated, which can be attributed to the magnetic nature of nanoparticles.

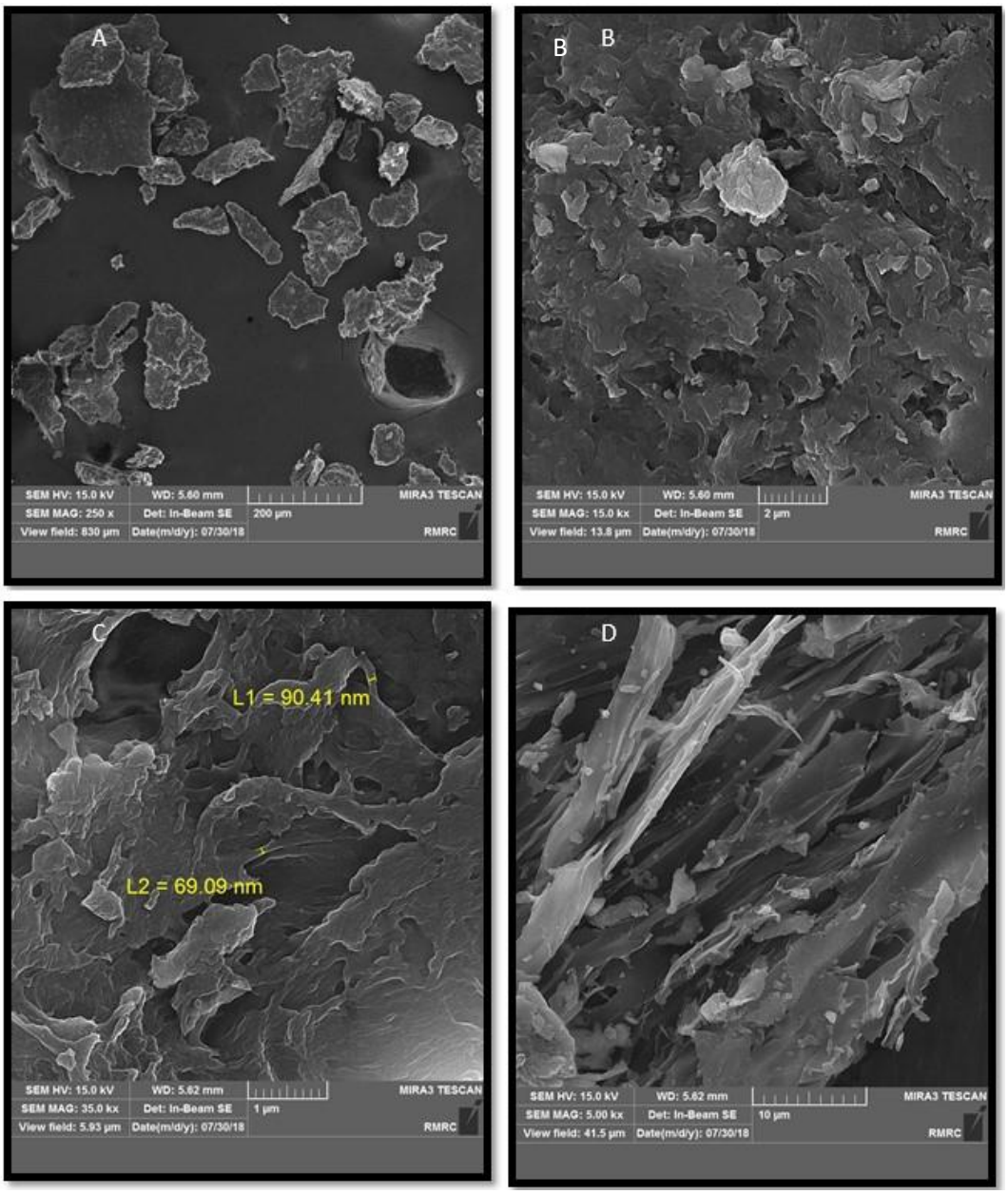

Fig. 3 – SEM image of magnetic hydrogel nanocomposite.

2. Effective parameters on the removal of Cu(II)

2.1. pH optimization

Effect of solution pH on Cu(II) adsorption on the magnetic hydrogel nanocomposite was studied at different pH (3.0–7.0). The pH of the solution is closely related to metal ion adsorption because the protonation and deprotonation of the adsorbent surface change with pH.[16,22] pH higher than 6.0 was not studied because at high pH, Cu(II) precipitation occurred.[16] According to the results shown in Fig. 4, the adsorption percentage increased until pH = 5 and then decreased. The decrease in the adsorption percentage at pH less than 5 is related to the high

concentration of H^+, followed by the protonation of the magnetic hydrogel nanocomposite and the decrease in the tendency to adsorb Cu(II).[23] Therefore, pH =5 was chosen for the next optimization steps.

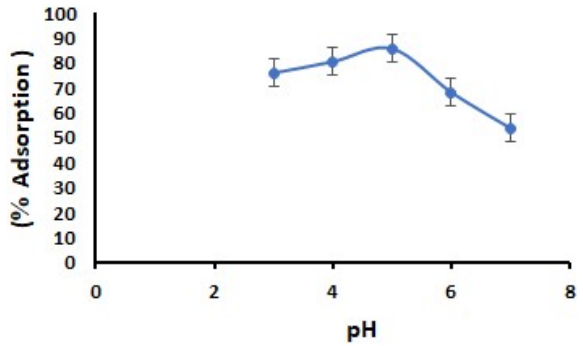

Fig. 4 – The percentage removal of Cu(II) in terms of pH.

2.2. Time effect

The sorption behaviors of the magnetic hydrogel nanocomposite for adsorbed of Cu(II) was studied at different contact times (15–90 min). The adsorption percentage of Cu(II) on the magnetic hydrogel nanocomposite increases with time and the equilibrium was attained in 60 min. As shown in Fig. 5, the adsorption percentage increased up to 60 min because the active sites were very accessible. Still, after the active sites were filled (saturated functional groups), the adsorption percentage was almost constant.[16,24]

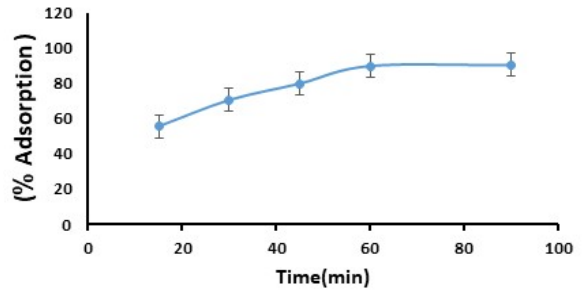

Fig. 5 – The percentage removal of Cu(II) in terms of contact time.

2.3. Adsorbent amount effect

To investigate the cost of the adsorption process, the amount of magnetic hydrogel nanocomposite was studied. Different magnetic hydrogel nanocomposite dose (0.05–0.03 g in 50 mL Cu(II) solution) was studied. As seen in Fig. 6, the adsorption percentage increased up to 0.2 mg of magnetic hydrogel nanocomposite amount because the active sites were increased and then remained almost constant. Similar results were obtained by Salehi *et al*.[16]

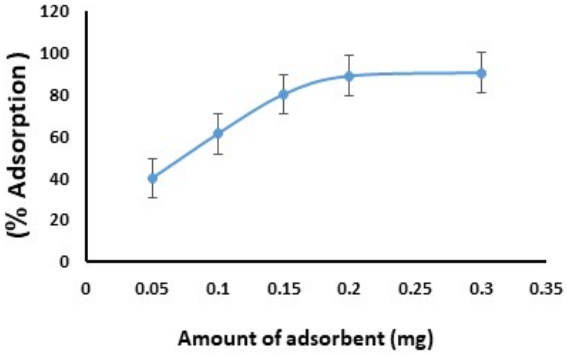

Fig. 6 – The percentage removal of Cu(II) in terms of magnetic hydrogel nanocomposite amount.

2.4. Sample volume effect

The effect of sample volume on the adsorption of Cu(II) by magnetic hydrogel nanocomposite was investigated in the range of 50–1000 mL of Cu(II) solution. Based on the results of Fig. 7, the metal ions were adsorbed up to 200 mL of the sample volume on the magnetic hydrogel nanocomposite. After 200 mL of the sample volume, the adsorption decreased significantly.

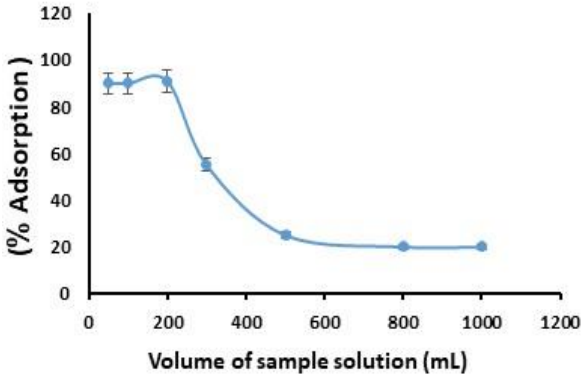

Fig. 7 – The percentage removal of Cu(II) in terms of Sample volume.

2.5. Interferences effect

To check the adsorption percentage in the presence of external ions, the adsorption percentage of copper (II) in the presence of some cations and anions was calculated. The results summarized in Table 1 indicated that the adsorption percentage of Cu(II) on the magnetic hydrogel nanocomposite was affected very little in the presence of interfering ions.

Table 1

The adsorption percentage of Cu(II) on the magnetic hydrogel nanocomposite in the presence of foreign ions

interfering ion	C metal ions / C interfering ion	% R
Na^+	100	90.3 (1.2)[a]
K^+	100	91.2 (1.3)
Ca^{2+}	100	90.8 (1.4)
Mg^{2+}	100	90.6 (1.6)
Cl^-	100	89.9 (1.0)
Br^-	100	92.0 (1.1)
Mn^{2+}	100	91.8 (1.2)
Zn^{2+}	100	90.7 (0.8)

[a] Values in parentheses are % RSD based on three individual replicate analyses

3. Reusability of the magnetic hydrogel nanocomposite

The reusability of the adsorbent has a significant effect on reducing the overall cost and its application in large and industrial scales. Therefore, adsorption and desorption were studied under optimal conditions. According to the result shown in Figure 8, the adsorption efficiency after five adsorption cycles and desorption of Cu(II) on the magnetic hydrogel nanocomposite with 5 mL of 1.0 M HNO_3 was acceptable stability.

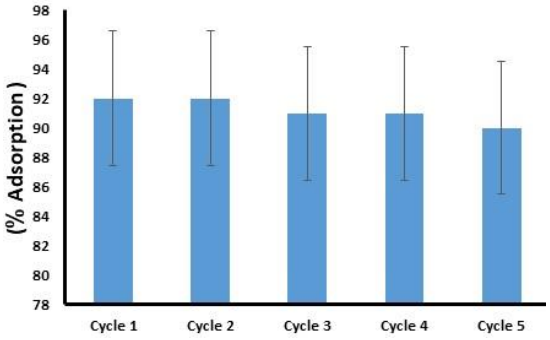

Fig. 8 – Reusability of magnetic hydrogel nanocomposite to absorb Cu(II).

4. Adsorption isotherms

The feasibility of adsorbing a sample with the desired adsorbent is checked by studying the adsorption isotherm. Therefore, the Langmuir, Freundlich and Temkin isotherm models were analyzed to fit the adsorption of copper (II) on magnetic hydrogel nanocomposite. The Langmuir isotherm model is represented by the following equation:

$$C_e/q_e = (1/K_L\, q_{max}) + (C_e/q_{max}) \qquad (3)$$

where C_e (mg/L) is the concentration of Cu(II) at equilibrium, q_m (mg/g) is the adsorption maximum of Langmuir model, K_L is the Langmuir constant.[25]

R_L (separation factor) is a dimensionless constant that is defined to describe the characteristics of the Langmuir model and is represented by the following equation:

$$R_{L=}\, 1/(1 + K_L\, C_0) \qquad (4)$$

R_L values indicate an unfavorable, favorable, or linear isotherm ($R_L > 1$, $0 < R_L < 1$ and $R_L = 1$, respectively).[26–28]

The Freundlich isotherms model is represented by the following equation:

$$ln\ q_e = ln\, K_F\ + 1/n(\, ln\, C_e) \qquad (5)$$

where K_F is the constant of the Freundlich model and n is the capacity and intensity of the adsorption.[25]

Tamkin's adsorption isotherm model assumes that the uniform distribution of binding energies decreases linearly with the heat of adsorption in these sites, which is represented by the following equation:

$$q_e = (BlnK_T) + (Bln\, C_e) \qquad (6)$$

where B is the adsorption heat, and K_T is the maximum binding energy.[22]

By comparing R^2 of isotherms (Table 2), the Langmuir isotherm model can be used to best describe Cu(II) adsorption behavior on the magnetic hydrogel nanocomposite. Therefore, the adsorption process of Cu(II) on the magnetic hydrogel nanocomposite is homogeneous and monolayer. Also, $0 < R_L < 1$ means favorable isotherm of Cu(II) on the magnetic hydrogel nanocomposite.

Table 2

Isotherm parameters for Cu(II) on the magnetic hydrogel nanocomposite

Isotherm model									
Langmuir				**Freundlich**			**Temkin**		
q_{max} (mg g^{-1})	K_L (L mg^{-1})	R_L	R^2	n	K_F (mg g^{-1}) (mg $L^{-1})^{-n}$	R^2	R^2	B (L g^{-1})	K_T
160.2	0.0248	0.2103	0.9978	2.69	21.03	0.9686	0.9669	2.89	2.01

5. Adsorption kinetics

Pseudo first and second order models were used to evaluate the experimental data of adsorption kinetics and calculated parameters. The linear model of pseudo-first and second-order models represent by the following equations (7) and (8), respectively:

$$1/q_t = (K_1/q_e\, t) + (1/q_e) \quad (7)$$

$$t/q_t = (1/K_2\, q_e^2) + (t/q_e) \quad (8)$$

where K_1 (1/min) is the pseudo-first-order rate constant, K_2 (g/(mg min)) is the constant of the pseudo-second-order rate and, q_t and q_e (mg/g) are the amount of Cu(II) adsorbed at time t at equilibrium.[25,29–32]

According to the results shown in Fig. 9 and Table 3, the pseudo-second-order model was better fitted with the experimental results. It can be concluded that the overall rate of Cu(II) adsorption on the magnetic hydrogel nanocomposite is controlled by pseudo-second-order kinetic. in fact, chemisorption is the rate-limiting step.[25,33]

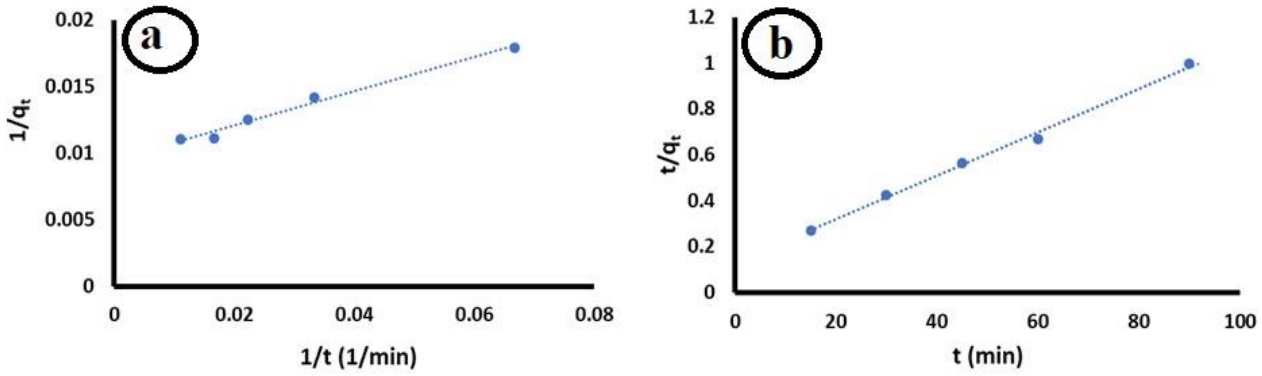

Fig. 9 – The pseudo-first-order model (a) and pseudo-second-order model of Cu(II) adsorption on the magnetic hydrogel nanocomposite.

Table 3

The parameters of adsorption kinetics for the adsorption of Cu(II) adsorption on the magnetic hydrogel nanocomposite

Pseudo-first order		**Pseudo-second order**	
q_e (mg/g)	0.66	q_e (mg/g)	3.98
k_1 (1/min)	0.08	k_2 (g/(mg min))	0.002
R^2	0.9855	R^2	0.9956

6. Thermodynamics studies

Thermodynamic parameters for adsorption of Cu(II) adsorption on the magnetic hydrogel nanocomposite such as ΔG° (kJ/mol), ΔH° (kJ/mol) and, ΔS° (kJ/mol K) at 303, 313, 323 and 333K were evaluated. According to the results shown in Table 4, ΔG° is negative at all temperatures, which indicates favorable spontaneous adsorption, and with increasing the temperature, the ΔG° value was decreased which indicates the adsorption was exothermic.[22] ΔS° was negative, which indicates a random decrease at the solid-solution interface of the magnetic hydrogel nanocomposite, and the ΔH° was also negative, which means physical and chemical adsorption in the adsorption process.[22, 34]

Table 4

Thermodynamic parameters for the adsorption of Cu(II) adsorption on the magnetic hydrogel nanocomposite

Temperature (K)	K_c	ΔG° (KJ/mol)	ΔH° (KJ/mol)	ΔS° (J/(mol K))
303.15(30°C)	3.97	–3.50	–25.65	–67.11
313.15(40°C)	2.62	–2.71		
323.15(50°C)	1.98	–1.75		
333.15(60°C)	1.85	–0.92		

7. Application on real samples

The results related to the adsorption efficiency of Cu(II) on the magnetic hydrogel nanocomposite in water and wastewater are summarized in Table 5. For this purpose, PET bottles were selected and washed with water, detergent solution, distilled water, and then dried.

The collected real samples included the Tehran tap water, Varamin Tap water and Charshahr factory effluent were filtered using a membrane filter to remove all suspended solids, and then their pH was adjusted to 6, and the adsorption efficiency of Cu(II) on the magnetic hydrogel nanocomposite was investigated under optimal conditions. As shown in Table 5, there is more Cu(II) in the sample of the Charshahr factory effluent and a small amount of Cu(II) in the Varamin Tap water, but there is no Cu(II) in the Tehran tap water sample. The percentage of recovery was higher than 98%, RSD (%) between 1.4–2.1%, and it shows that the proposed method is able to remove Cu(II) by magnetic hydrogel nanocomposite in real samples.

Table 5

Application of the magnetic hydrogel nanocomposite to removal of Cu(II) in real samples

Samples	Added Cu(II) (μg)	GF-AAS method	t_{exp}
Tehran tap water	0	N.D[a]	–
	10.00	10.03 (2.1)[b]	1.46
Varamin Tap water	0	4.94 (1.3)	–
	10.00	14.75 (1.4)	1.7
Charshahr factory effluent	0	85.15 (1.5)	–
	10	95.10 (1.4)	1.43

[a] Not Detected
[b] Values in parentheses are % RSD based on three individual replicate analyses

8. Paired t-test

The results of the removal of Cu(II) by the magnetic hydrogel nanocomposite and determination by GF-AAS and ICP Spectroscopy were applied in the T-test, and amounts of t_{exp} are given inthe Table 5. Based on the results, there was no significant difference between GF-AAS and ICP Spectroscopy methods. So it can be said that GF-AAS and ICP Spectroscopy methods can be used to determine Cu(II) in water and waste water samples.

9. Comparison of the adsorption efficiency of Cu(II) by various methods

The contact time and q_{max} of Cu(II) for different methods were compared with the proposed method. The results summarized in Table 6 show that the proposed method is fast due to its short equilibrium time (60 min) and has a high adsorption capacity (160.2 mg/g) compared to other methods for Cu(II) removal.[23,35–38] Similar contact time was observed in Poly (Acrylic Acid/Acrylamide) Hydrogel and Magnetic chitosan/cellulose microspheres adsorbent but the proposed magnetic hydrogel nanocomposite had better adsorption capacity.

Table 6

Comparison of the adsorption efficiency of Cu(II) by various methods

Adsorbent	q_{max} (mg/g)	Contact time (min)	Ref.
Magnetic chitosan modified with cysteine-glutaraldehyde	156.49	90	[23]
Poly (Acrylic Acid/Acrylamide) Hydrogel	159.45	60	[35]
Fe_3O_4-CS-L	156.49	90	[36]
Magnetic chitosan/cellulose microspheres	88.21	60	[37]
Chitosan/sporopollenin microcapsules	84.42	240	[38]
magnetic hydrogel nanocomposite	160.2	60	This work

* Data not reported.

CONCLUSION

In this study, XG modified with Fe_3O_4 nanoparticles and polyacrylamide and polyacrylic acid as a homopolymer, and therefore the functional groups of XG, its mechanical resistance and surface area was improved to removal of Cu(II) in water and waste water samples and then determined using GF-AAS. The adsorbent was magnetic, so the separation was speedy and simple because we didn't need to centrifuge or purify the sample. The parameters related to isotherm models were calculated and it was found the Langmuir isotherm model can be used to best describe Cu(II) adsorption behavior on the magnetic hydrogel nanocomposite. So, adsorption process of Cu(II) on the magnetic hydrogel nanocomposite homogeneous and monolayer. The overall rate of Cu(II) adsorption on the magnetic hydrogel nanocomposite is controlled by pseudo-second-order kinetic, and in fact, chemisorption is the rate-limiting step. $\Delta G°$ was negative, showing that favorable spontaneous adsorption; $\Delta S°$ was negative, showing that a random decrease at the solid-solution interface of the magnetic hydrogel nanocomposite; and the $\Delta H°$ was also negative, showing that physical and chemical adsorption in the adsorption process. The adsorption efficiency after five cycles of adsorption and desorption of Cu(II) on the magnetic hydrogel nanocomposite with 5 mL of 1.0 M HNO_3 was acceptable stability. Finally, the magnetic hydrogel nanocomposite exhibited high performance in removing the Cu(II) from water and wastewater samples.

REFERENCES

1. J. Wen and X. Hu, *J. Colloid. Interface. Sci.*, **2021**, *589*, 578–586.
2. S. A. El-Kholy, E. K. Radwan, M. E. El-Naggar, S. T. El-Wakeel and I. El-Tantawy El Sayed, *J. Environ. Chem. Eng.*, **2023**, *11*, 110652–110658.
3. L. Wang, D. Hu, X. Kong, J. Liu, X. Li, K. Zhou, H. Zhao and C. Zhou, *J. Chem. Eng.*, **2018**, *346*, 38–49.
4. F. L. Fu and Q. Wang, *J. Environ. Manag.*, **2011**, *92*, 407–418.
5. L. Mo, S. Zhang, F. Qi and A. Huang, *Int. J. Biol. Macromol*., **2022**, *209*, 1922–1932.
6. A. Safdarian and V. Javanbakht, *Int. J. Biol. Macromol*., **2024**, *261*, 129729–129736.
7. R. M. Gohari, M. Safarnia, A. D. Koohi and M. B. Salehi, *Chem. Eng. Res. Des*., **2022**, *188*, 714–728.
8. A. Rahmatpour, A. H. A. Hesarsorkh, *Carbohydr. Polym*., **2024**, *328*, 121721–121728. DOI: 10.1016/j.carbpol. 2023.121721.
9. H. Zhang, T. Lou and X. Wang, *J. Water Proc. Engineering*., **2023**, *56*, 104455–104460. DOI:10.1016/j. jwpe.2023.104455.
10. E. M. Nsengiyumva and P. Alexandridis, *Int. J. Biol. Macromol*., **2022**, *216*, 583–604.
11. S. Liu, F. Yao, O. Oderinde, Z. Zhang and G. Fu, *Carbohydr. Polym*., **2017**, *174*, 392–399.
12. M. A. Jalali, A. D. Koohi and M. Sheykhan, *Carbohydr. Polym*., **2016**, *142*, 392–399.
13. H. Mittal, V. Parashar, S. B. Mishra and A. K. Mishra, *Chem. Eng. J*., **2014**, *255*, 471–482.
14. R. R. M. dahaji, A. Moghimi, H. Faraji and F. Azizinejad, *Rev. Roum. Chim*., **2023**, *68*, 495–505.
15. H. X. Che, S. P. Yeap, A. L. Ahmad and J. K. Lim, *Chem. Eng. J*., **2014**, *243*, 68–78.
16. N. Salehi, A. Moghimi and H. Shahbazi, *Int. J. Environ. Anal. Chem*., **2022**, *102*, 2305–2321.
17. R. Sardari and N. Osouleddini, *Data in brief*, **2018**, *19*, 1794–1798.
18. A. Moghimi, *Russ. J. Phys. Chem. A*., **2013**, *87*, 1203–1209.
19. S. Özdemira, S. A. Mohamedsaid, E. Kılınçc and M. Soylak, *Food. Chem*., **2019**, *271*, 232–238.
20. R. Jindal, B. S. Kaith, H. Mittal and S. Berry, *Polym. Renew. Resour*., **2013**, *4*, 19–34.
21. B. Xiang, D. Ling, H. Lou and H. Gu, *J. Hazard. Mater*., **2017**, *325*, 178–188.
22. M. P. Arvand, A. Moghimi and N. Salehi, *Environ. Monit. Assess*., **2024**, *196*, 136. DOI:10.1007/s10661-023-12149-x.
23. Y. G. A. El-Reash, *J. Chem. Eng*., **2016**, *4*, 3835. DOI:10.1016/j.jece.2016.08.014.
24. N. Salehi, A. Moghimi and H. Shahbazi, *IET. Nanobiotechnology*., **2021**, *15*, 575–584.
25. S. Zhang, F. Xu, Y. Wang, W. Zhang, X. Peng and F. Pepe, *Chem. Eng. J*., **2013**, *234*, 33–39. DOI:10.1016 /j.cej.2013.08.102.
26. A. Z. M. Badruddoza, Z. B. Z. Shawon, T. W. J. Daniel, K. Hidajat and M. S. Uddin, *Carbohydr. Polym*., **2013**, 91, 322–332.
27. R. Ahmad and A. Mirza, *ISGSD*., **2018**, *7*, 101–108.

28. M. Abniki and A. Moghimi, *Mater. Chem. Phys*., **2024**, *316*, 129117–129124. DOI: 10.1016/j.matchemphys.2024.129117.
29. S. S. Abdullaev, F. Al-dolaimy, A. H. Alawadi, A. T. Alkhafaji, J. Zareei and S. H. Hosseini, *Heliyon*, **2023**, *9*, e22761. DOI: 10.1016/j.heliyon.2023.e22761.
30. N. Salehi and A. Moghimi, *Polym.-Plast. Technol. Mater*., **2024**. DOI:10.1080/25740881.2024.2351558.
31. R. C. Bevilacqua, I. A. Preigschadt, M. S. Netto, J. Georgin, D. S. P. Franco, E. S. O. Mallmann, L. F. Silva, D. Pinto, E. L. Foletto and G. L. Dotto, *J. Environ. Sci. Health B*., **2021**, *26*, 995–1006.
32. M. Abniki and A. Moghini, *Mater. Chem. Physics*., **2024**, *316*, 129117. https://doi.org/10.1016/j.matchemphys.2024.129117.
33. C. Y. Lee, T. Kim, S. Komarneni and S.-K. Han, Cho, *Appl. Clay Sci*., **2013**, *83-84*, 263–269.
34. S. Joshi and R. K. Srivastava, *Environ. Monit. Assess*., **2019**, *191*, 615–624. DOI: 10.1007/s10661-019-7777-5.
35. Y. Ling-Yun, L. Rui-Li, W. Hai-Lun, Z. Shan-Fa, C. Min-Wei, S. Xiao-Xue, H. Mei and L. Hai, *Chinese J. Anal. Chem*., **2020**, *48*, e20098–e20106. DOI: 10.1016/S1872-2040(20)60037-8.
36. I. V. Joseph, L. Tosheva and M. Doyle, *J. Environ. Chem. Engin*., **2020**, *8*, 103895–103904. DOI: 10.1016/j.jece.2020.103895.
37. X. Luo, J. Zeng, Sh. Liu and L. Zhang, *Bio. Tech*., **2015**, *194*, 403–409. DOI: 10.1016/j.biortech.2015.07.044.
38. I. Sargına and G. Arslan, *Int. J. Bio. Macromol*., **2015**, *75*, 230–238.